RSC Advances

PAPER

View Article Online
View Journal | View Issue

Cite this: *RSC Adv.*, 2015, **5**, 34645

$ZnO/Ag/Mn_2O_3$ nanocomposite for visible light-induced industrial textile effluent degradation, uric acid and ascorbic acid sensing and antimicrobial activity†

R. Saravanan,*[af] Mohammad Mansoob Khan,[b] Vinod Kumar Gupta,[cde] E. Mosquera,[f] F. Gracia,[a] V. Narayanan[g] and A. Stephen*[h]

A facile and inexpensive route has been developed to synthesize a ternary $ZnO/Ag/Mn_2O_3$ nanocomposite having nanorod structures based on the thermal decomposition method. The as-synthesized ternary $ZnO/Ag/Mn_2O_3$ nanocomposite was characterized and used for visible light-induced photocatalytic, sensing and antimicrobial studies. The ternary $ZnO/Ag/Mn_2O_3$ nanocomposite exhibited excellent and enhanced visible light-induced photocatalytic degradation of industrial textile effluent (real sample analysis) compared to pure ZnO. Sensing studies showed that the ternary $ZnO/Ag/Mn_2O_3$ nanocomposite exhibited outstanding and improved detection of uric acid (UA) and ascorbic acid (AA). It also showed effective and efficient bactericidal activities against *Staphylococcus aureus* and *Escherichia coli*. These results suggest that the small size, high surface area and synergistic effect among ZnO, AgNPs and Mn_2O_3 induced visible light photocatalytic activity by decreasing the recombination of photogenerated electrons and holes, and extending the response of pure ZnO to visible light, enhanced sensing of UA and AA and antimicrobial activity. Overall, the ternary $ZnO/Ag/Mn_2O_3$ nanocomposite is a valuable material that can be used for a range of applications, such as visible light-induced photocatalysis, sensing and antimicrobial activity. Therefore, ternary nanocomposites could have important applications in environmental science, sensing, and biological fields.

Received 10th February 2015
Accepted 8th April 2015

DOI: 10.1039/c5ra02557e

www.rsc.org/advances

Introduction

Water is considered as the elixir of life because the world would not have any life without water. It is essential for every living organism, but the quantity and quality of water is insufficient and inappropriate in accomplishing the needs of human beings. The amount of fresh water on earth is inadequate for human beings in fulfilling their requirements. The amount of waste water is increasing with the rapid growth of industrialization. The United Nations has stated that the yearly amount of waste water produced is six times more than that of all the existing rivers of the world.[1,2] Thus, water pollution creates major environmental issues around the globe. Hence, pollution treatment should be a major concern. On the other hand, removal of pollutants from waste water can be achieved by several methods.[3] One of the best and green environmentally friendly methods is photocatalysis. It is an attractive and efficient way to solve the above issue by a cost effective approach. In the recent years, nanomaterials are utilized for various applications because of novel characteristics. Specially, nano-semiconducting materials which are used for photocatalysis and biosensors owing to their applications in degrading industrial pollutants and highly sensitive detection of various enzymes. They have significant impact on human health and the ecosystem.[4–12]

Biosensors are being used in the detection of innumerable enzymes and chemicals at very low detection limit. Among the various enzymes and chemicals, the detection of uric acid (UA)

[a]*Department of Chemical Engineering and Biotechnology, University of Chile, Beauchef 850, Santiago, Chile. E-mail: saravanan3.raj@gmail.com; Fax: +56-2-699-1084; Tel: +56-2-978-4284*

[b]*Chemical Sciences, Faculty of Science, Universiti Brunei Darussalam, Jalan Tungku Link, BE1410, Brunei Darussalam*

[c]*Department of Chemistry, Indian Institute of Technology Roorkee, Roorkee, 247 667, India*

[d]*Center for Environment and Water, The Research Institute, King Fahd University of Petroleum and Minerals Dhahran, Saudi, Saudi Arabia*

[e]*Department of Applied Chemistry, University of Johannesburg, Johannesburg, South Africa*

[f]*Nanoscale Materials Laboratory, Department of Materials Science, University of Chile, Avenida Tupper 2069, Santiago, Chile*

[g]*Department of Inorganic Chemistry, University of Madras, Guindy Campus, Chennai, 600 025, India*

[h]*Department of Nuclear Physics, University of Madras, Guindy Campus, Chennai, 600 025, India. E-mail: stephen_arum@hotmail.com; Tel: +91-44-22202802*

† Electronic supplementary information (ESI) available: FE-SEM & EDS of all the prepared catalysts and procedure for antimicrobial activity. See DOI: 10.1039/c5ra02557e

and ascorbic acid (AA) is of utmost importance which plays a significant role in human beings health. A small variation in the standard level of UA as well as AA creates a lot of diseases to human beings. Therefore, to find the level of UA and AA at earlier stage is necessary.[13–15] Among the various analytical methods, electrochemical analysis has been proven to be a very promising approach for UA and AA detection.[13–15] Among the metal oxides, zinc oxide (ZnO) nanomaterials has been broadly used as biosensor and photocatalytic material due to their low cost, biocompatibility, and chemical stability against photocorrosion and chemical corrosion.[13,14,16] Ahmad *et al.* described the effective determination of uric acid with a detection limit of 0.05–2 mM using ZnO nanosheets which were found to provide high electron flow, thus favouring enhanced sensitivity.[17] Xia *et al.* proposed that glassy carbon electrodes modified with hierarchical ZnO nanoflowers showed an enhanced sensitivity with a very low electrochemical detection limit for dopamine.[18]

However, photodegradation of the pollutants using ZnO is restricted under visible light because of the large band gap. Thus, significant efforts have been directed towards the research on suitable visible light driven catalysts that is one of the major challenging issue. Different materials and techniques were used to functionalize the ZnO to degrade the pollutants under visible light irradiation.[19–25] Recently, it was reported that, the synergistic coupling effect between ZnO and Mn_2O_3 system effectively prevents the electron–hole recombination that results the degradation of textile effluent in 8 h under visible light irradiation.[25] Saravanan *et al.* reported that the surface modification of the ZnO by Ag acts as an electron–hole separation center, hence, enhances the photocatalytic activity. In particular, ZnO/Ag (90 : 10) system has shown higher photocatalytic activity compared with other weight percentages and it was successfully used for the degradation of textile dyes in 4 h under visible light irradiation.[24]

This paper reports the synthesis of a novel ternary ZnO/Ag/Mn_2O_3 nanocomposite with improved photodegradation efficiency in a short interval of visible light irradiation. The ternary ZnO/Ag/Mn_2O_3 nanocomposite was prepared in the ratio of (80 : 10 : 10) using facile thermal decomposition method. The synthesized catalyst was characterized by different techniques and used for multiple applications such as the photocatalytic degradation of industrial textile effluents (real sample analysis) under visible light irradiation, electrochemical detection of UA and AA and antimicrobial activities. To the best of the author's knowledge, no research reports have been published on the photocatalytic degradation of the industrial textile effluent as well as UA and AA sensing using ternary ZnO/Ag/Mn_2O_3 nanocomposite. It was also used for antimicrobial activity against *Staphylococcus aureus* and *Escherichia coli*. The as-prepared ternary ZnO/Ag/Mn_2O_3 nanocomposite showed enhanced visible light-induced photocatalytic activity, UA and AA sensing and antimicrobial activity in comparison to pure ZnO.

Experimental

Materials

All the required chemicals such as zinc acetate dihydrate, silver acetate, manganese(II) acetate tetrahydrate, uric acid (UA) and ascorbic acid (AA) were purchased from Sigma-Aldrich. All the aqueous solutions were prepared using double distilled (DD) water.

Methods

The crystal structure of the synthesized samples were confirmed by powder X-ray diffractometer at room temperature (Rich Seifert 3000, Germany) using Cu $K_{\alpha 1}$ radiation ($\lambda = 1.5406$ Å) in a wide range of Bragg angles (2θ, in the range of 10–70°) with a step size of 0.01. Field emission scanning electron microscopy (FE-SEM, HITACHI-SU6600, Hitachi, Japan) and energy dispersive X-ray spectroscopy (EDX) analysis were used to find morphology and the elements present in the catalysts. The specific surface area of the catalysts were calculated using Brunauer–Emmett–Teller (BET, Micromeritics ASAP 2020, USA). The analysis procedure is fully automated and operates with the static volumetric technique. Before each measurement, the samples (100 mg) were pre-treated by N_2 at 120 °C for 1 h. The surface oxidation states of the catalysts were studied using X-ray photoelectron spectroscopy (XPS, DRA 400 – XM1000 OMICRON, ESCA$^+$, Omicron Nanotechnology, Germany). The XPS spectra were collected using Omicron ESCA spectrometer with monochromatized Al K_α radiation operating at 150 W. The catalyst specimens were prepared by pressing powder samples to a small pellet, followed by the base pressure (10^{-9} Torr) of the instrument. High-resolution spectra were collected at fixed analyzer pass energy at 20 eV. Binding energies were referenced to the C 1s binding energy of adventitious carbon contamination which was set at 284.6 eV. Shape and morphology of the samples were analyzed using a transmission electron microscope (TEM, Mark II, JEOL 2000FX, Tokyo, Japan), operated at 200 kV. The scanning transmission electron microscope (STEM) and elemental mapping were carried out by Tecnai F20-FEI, USA. The optical reflectance spectra were obtained using a UV-VIS-NIR Spectrophotometer (VARIAN CARY 5E, USA). The photocatalytic activity was measured by UV-visible spectrophotometer (RX1, Perkin-Elmer, USA). Degradation of industrial textile effluent was confirmed by total organic content (TOC) which was carried out using TOC analyser (Shimadzu TOC analyser, Japan).

Synthesis of catalysts

Pure ZnO nanomaterial was synthesized as per our previous reports.[23–26] In short; 3.0 g of the zinc acetate dihydrate was grounded for 3 h using a mortar and pestle. Grounded material was taken in an alumina crucible and calcined at 350 °C for 3 h in a muffle furnace. Similarly, ZnO/Ag/Mn_2O_3 nanocomposite was synthesized by mixing various weight percentages of zinc acetate dihydrate, silver acetate, and manganese(II) acetate tetrahydrate (80 : 10 : 10). The mixture was grounded for 3 h and calcined at 350 °C for 3 h.

Photocatalytic experiments

A projection lamp (7748XHP 250 W, Philips) is used as a source of visible light in a photoreactor. A 0.5% aqueous $K_2Cr_2O_7$

solution was circulated in a glass jacket of 600 mL cylindrical beaker which prevents the UV-rays. The industrial textile effluent was collected from dye industries (Tirupur, Tamilnadu, India). To reduce the turbidity of the industrial textile effluent, 50 mL of the textile effluent was diluted with 450 mL of distilled water (1 : 9 ratio). In this photocatalytic reaction, 500 mg of the catalyst was mixed with 500 mL of diluted industrial textile effluent followed by sonication for 10 min in the dark. The solutions were again stirred in the dark for 30 min to complete the adsorption and desorption equilibrium on the catalysts. Visible light irradiations of the solutions were performed. The irradiated samples were collected at regular intervals of time, centrifuged and filtered. Further, the filtered samples were analyzed using UV-visible spectrophotometer.

Electrochemical experiments

All the electrochemical measurements were performed on PGSTAT-12 electrochemical work station, (AUTOLAB, The Netherlands BV). The measurements were based on a three electrode system having a glassy carbon electrode (GCE) (0.07 cm^2), Pt wire (~20 cm^2), and saturated calomel electrode (SCE) which were used as working, counter, and reference electrodes respectively. Prior to each experiment, GCE surface was polished with finer grade alumina powder down to mirror polish, sonicated for about 15 min in DD water, degreased with acetone and washed with copious amount of DD water. All the solutions were purged with nitrogen (99.99%) for at least 30 min prior to each electrochemical measurement and an inert environment was maintained throughout the experiments. Pure ZnO and ternary ZnO/Ag/Mn_2O_3 nanocomposite was used to modify the GCE as follows: 3.0 mg of pure ZnO and ternary ZnO/Ag/Mn_2O_3 nanocomposite was separately suspended in 3 mL of ethanol and sonicated for 30 min in order to obtain a homogeneous suspension. Cleaned, polished and dried GCE was coated with 5 μL of the above suspensions to obtain pure ZnO and ternary ZnO/Ag/Mn_2O_3 nanocomposite modified GCE.

Results and discussion

In this study, synthesis of pure ZnO and ternary ZnO/Ag/Mn_2O_3 nanocomposite was based on the vapor to solid mechanism using a facile thermal decomposition method.[27] Raising the temperature of the raw materials, results in the formation of their vapours which upon cooling gets settled down/deposited on the crucible. In the beginning of condensation, defects on the surface of the substrate (crucible) acts as favourable sites for nucleation of the oxide vapours.[27] Further condensation of vapors allows such nuclei to grow into nanoparticles. This method is simple and cost effective compared to other methods. In the present study, for the first time, it has been shown that the ternary ZnO/Ag/Mn_2O_3 nanocomposite has effectively degraded the industrial textile effluent, used for detection and antimicrobial activities.

Fig. 1a shows the X-ray diffraction patterns of pure ZnO at 2θ values of 32.15°, 34.77°, 36.61°, 47.90°, 56.84°, 63.10°, 68.15°, and 69.31° which corresponds to the (h k l) planes (100), (002),

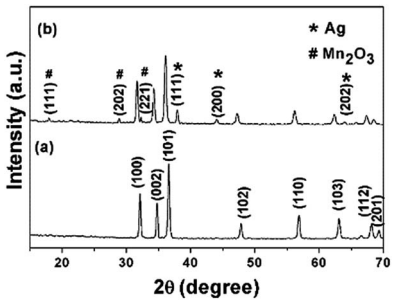

Fig. 1 XRD patterns of the synthesized (a) pure ZnO and (b) ternary ZnO/Ag/Mn_2O_3 nanocomposite.

(101), (102), (110), (103), (112), and (201) respectively. The XRD data of pure ZnO exhibited hexagonal structure (JCPDS no.: 79-0208) without any impurities. The XRD pattern of the synthesized ternary ZnO/Ag/Mn_2O_3 nanocomposite is shown in Fig. 1b. All the diffraction peaks are indexed and their result proves that the addition of impurity (silver and manganese) does not affect the ZnO structure. Fig. 1b illustrates the ZnO diffraction peaks along with (111), (200), (202) planes which represented the cubic structure of Ag (JCPDS no.: 89-3722) and (111) (202), (221) planes for a monoclinic structure of Mn_2O_3 (JCPDS no.: 06-0540). Hence, the XRD results clearly show the formation of ternary ZnO/Ag/Mn_2O_3 nanocomposite without any other impurities.

The morphology of the synthesized pure ZnO and ternary ZnO/Ag/Mn_2O_3 nanocomposite were analysed using FE-SEM and their consistent images are shown by Fig. S1a.† The FE-SEM analysis of pure ZnO shows nanorods which are randomly oriented. The diameter of the nanorods are around

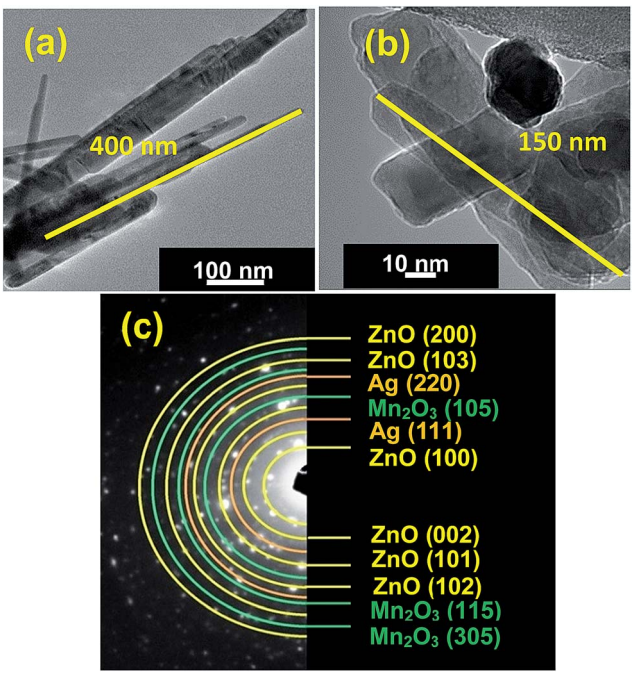

Fig. 2 TEM images of (a) pure ZnO, (b) ZnO/Ag/Mn_2O_3 and (c) SAED pattern of ternary ZnO/Ag/Mn_2O_3 nanocomposite.

40–50 nm and their lengths are in micrometre range. The FE-SEM analysis of ternary ZnO/Ag/Mn_2O_3 nanocomposite is represented by Fig. S1b.† From the close observation, the image specifies the small size of nanorods along with nanoparticles. The addition of silver and manganese oxide may influence the size and morphology of pure ZnO. The purity of the synthesized samples were confirmed by EDX analysis shown by Fig. S2.† The EDX spectra shows the presence of Zn and O in case of pure ZnO; and Zn, O, Ag, and Mn in case of ZnO/Ag/Mn_2O_3 nanocomposite. No any other impurities were observed in EDX analysis.

Further structure and morphology of the synthesized pure ZnO and ternary ZnO/Ag/Mn_2O_3 nanocomposite were confirmed by TEM analysis. Fig. 2a shows TEM image of pure ZnO which clearly represents nanorods which are randomly distributed whose lengths and diameters are in the range of 400–600 and 40–50 nm respectively. In case of ternary ZnO/Ag/Mn_2O_3 nanocomposite HRTEM image is epitomized by Fig. 2b. The results of HRTEM is similar to the FE-SEM results, which also shows small size of nanorods along with some nanoparticles. It is clearly observed that the size of the nanorods decreases (150–200 nm) because of the heterogeneous nucleation and synergistic effect in ternary ZnO/Ag/Mn_2O_3 nanocomposite.[28–30] The selected area electron diffraction (SAED) pattern of the ternary ZnO/Ag/Mn_2O_3 nanocomposite is shown by Fig. 2c which illustrates that there are several electron diffraction rings. The *d*-spacing values of the rings are indexed and their corresponding (*h k l*) planes were identified. The result of the SAED pattern is in close agreement with the XRD results. The planes are matched with a hexagonal structure of ZnO (JCPDS no.: 79-0208), cubic structure of Ag nanoparticles (JCPDS no.: 89-3722) and monoclinic structure of Mn_2O_3 (JCPDS no.: 06-0540). The location of different particles in the ternary ZnO/Ag/Mn_2O_3 nanocomposite were identified by STEM analysis and their corresponding bright and dark field images are shown by Fig. S3.† Using this (highlighted square box), elemental mapping (Fig. S4†) was performed and results clearly represents that in the ternary ZnO/Ag/Mn_2O_3 nanocomposite ZnO, Ag and Mn_2O_3 were distributed uniformly and not segregated individually. This confirms the formation of ternary ZnO/Ag/Mn_2O_3 nanocomposite.

BET measurements were performed to find the specific surface area of the pure ZnO and ternary ZnO/Ag/Mn_2O_3 nanocomposite which was 8.7 $m^2\ g^{-1}$ and 17.3 $m^2\ g^{-1}$ respectively, which is in agreement with the TEM results. It was found that the surface area of the ternary ZnO/Ag/Mn_2O_3 nanocomposite is almost twice compared to the pure ZnO. The result of TEM was further supported by the BET measurements. The specific surface area of ternary ZnO/Ag/Mn_2O_3 nanocomposite has increased because of the synergistic and nucleation effect.[28–31] The pure ZnO nanorods easily grows whereas in the case of ternary ZnO/Ag/Mn_2O_3 nanocomposite, the addition of silver and manganese oxide prevents the growth of ZnO nanorods. These consequences suggest that there is a synergetic effect among the Ag, Mn_2O_3 and ZnO in the ternary ZnO/Ag/Mn_2O_3 nanocomposite. According to Wang *et al.* silver loaded to ZnO/SnO_2 system exhibit high surface area and enhance the photocatalytic activity.[30] Similarly, potassium incorporation into Cu/TiO_2 materials show greater surface area and better catalytic performance.[31] Optimized amount of copper supported on the CeO_2/TiO_2 oxides provides high surface area and superior catalytic performance than copper supported on CeO_2 or TiO_2.[32] Hence, the ternary ZnO/Ag/Mn_2O_3 nanocomposite having small size and high surface area might provide higher photocatalytic activities.

The oxidation states and surface components of the ternary ZnO/Ag/Mn_2O_3 nanocomposite was identified by XPS analysis. The surface of ternary ZnO/Ag/Mn_2O_3 nanocomposite consists of Zn, Ag, Mn, O and C which is confirmed by survey spectrum shown by Fig. 3a. The high resolution XPS spectrum of Zn is represented by Fig. 3b. The binding energies at 1021.5 and 1044.2 eV for $2p_{3/2}$ and $2p_{1/2}$ of Zn^{2+} states are consistent with the previous report.[22] Fig. 3c shows the high resolution XPS spectrum of silver which exhibits Ag $3d_{5/2}$ and Ag $3d_{3/2}$ peaks at 367.5 eV and 373.5 eV. The Mn $2p_{3/2}$ and Mn $2p_{1/2}$ peaks exist at binding energies of 641.3 eV and 654.1 eV (Fig. 3d) which confirms the presence of Mn^{3+} in the ZnO/Ag/Mn_2O_3 nanocomposite. Fig. 3e illustrates the high resolution O 1s fitted XPS spectrum which indicates the presence of three types of oxygen in the ternary ZnO/Ag/Mn_2O_3 nanocomposite at the binding energy of 529.2, 531.5 and 534.1 eV for pure ZnO, Mn_2O_3 and surface hydroxyl groups respectively.[33]

The optical band gap energy of the prepared samples were investigated using UV-vis diffuse reflectance spectra (DRS). Fig. 4a shows DRS spectra of pure ZnO and ternary ZnO/Ag/Mn_2O_3 nanocomposite. Fig. 4a clearly showed that the prepared pure ZnO has a strong edge absorption in the UV region, while the ternary ZnO/Ag/Mn_2O_3 nanocomposite shows the absorption in the visible region. The variation of edge absorption

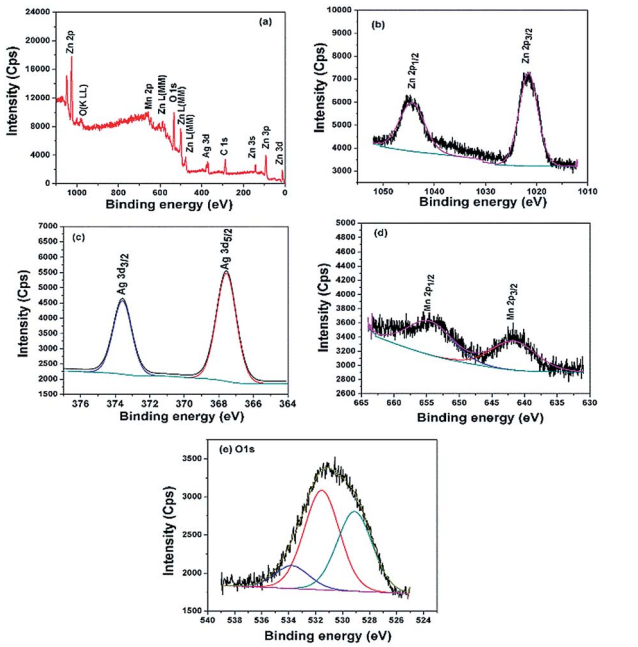

Fig. 3 XPS spectra of ternary ZnO/Ag/Mn_2O_3 nanocomposite (a) survey, (b) zinc, (c) silver, (d) manganese and (e) oxygen.

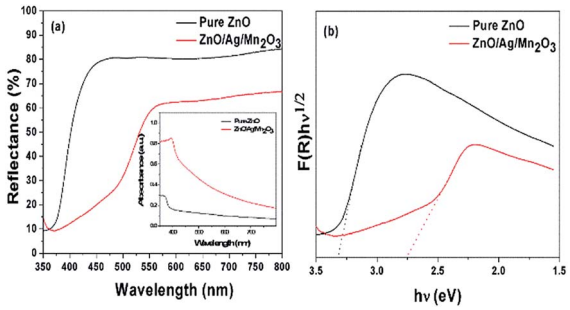

Fig. 4 (a) UV-vis diffuse reflectance spectra, and the inset shows UV-vis absorption spectra, and, (b) $F(R)h\nu^{1/2}$ *vs.* $h\nu$ plot of the pure ZnO and ternary ZnO/Ag/Mn_2O_3 nanocomposite.

arises because of the synergetic effect between ZnO, Ag and Mn_2O_3.[30] Based on Kubelka–Munk relation, the intercept of the plot between $(F(R)h\nu)^{1/2}$ *vs.* $h\nu$ (Fig. 4b) provides the band gap energy of the prepared materials. The band gap energy obtained for pure ZnO and the ternary ZnO/Ag/Mn_2O_3 nanocomposite is 3.31 and 2.75 eV respectively. It is known that the photocatalytic process mainly depends on wavelength of irradiated light. So the photocatalytic process in case of the ternary ZnO/Ag/Mn_2O_3 nanocomposite could be better under visible light irradiation because of the reduced band gap.

Photocatalytic degradation of industrial textile effluent

Photocatalytic degradation activity of pure ZnO and ternary ZnO/Ag/Mn_2O_3 nanocomposite were studied by degrading the industrial textile effluent under visible light irradiation. Fig. 5a represents the decrease in the absorption spectra of industrial textile effluent after degradation using ternary ZnO/Ag/Mn_2O_3 catalyst. Increase in irradiation time brought a decrease in the absorption band as evident from Fig. 5a. Most of the industrial textile effluents have been degraded within 3 h using ternary ZnO/Ag/Mn_2O_3 catalyst under visible light irradiation. Time course degradation curves for industrial textile effluents using pure ZnO and ternary ZnO/Ag/Mn_2O_3 catalyst is shown in Fig. 5b. It was found that the ternary ZnO/Ag/Mn_2O_3 nanocomposite exhibited 96.9% catalytic activity. The inset of Fig. 5b

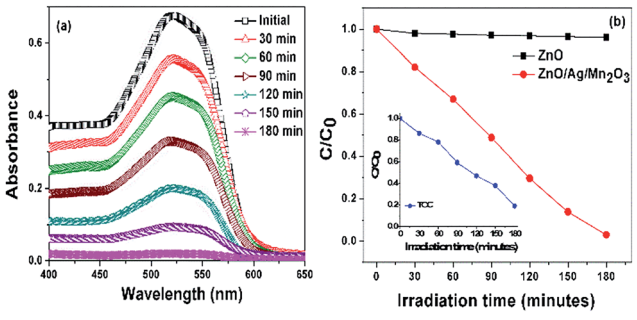

Fig. 5 (a) UV-vis absorbance spectra, and, (b) time course degradation curves of industrial textile effluents using pure ZnO and ternary ZnO/Ag/Mn_2O_3 nanocomposite and inset shows TOC result under visible light irradiation.

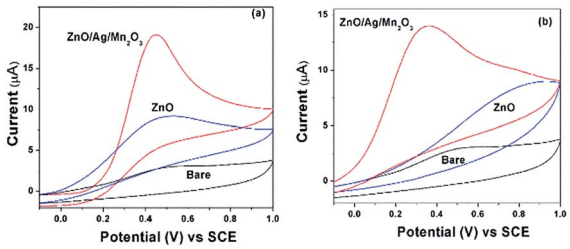

Fig. 6 The CV results of bare GCE and pure ZnO nanorods as well as ternary ZnO/Ag/Mn_2O_3 nanocomposite modified GCE in presence of 3 mM (a) UA and (b) AA.

represents TOC result for industrial textile effluent degradation by ternary ZnO/Ag/Mn_2O_3 nanocomposite. This confirms that as the irradiation time is increasing, the concentration of industrial textile effluent is decreasing which is attributed to its complete degradation. On the other hand, pure ZnO owing to its large band gap did not show any degradation of industrial textile effluent. The recycling ability (Fig. S5†) of ternary ZnO/Ag/Mn_2O_3 nanocomposite was carried out to find the stability of the materials. After undergoing recycling process of industrial textile effluent for five times under visible light irradiation, only slight variation was found. Thus, it is concluded that the ternary ZnO/Ag/Mn_2O_3 nanocomposite exhibits good stability and reusability. In our previous work, ZnO/Mn_2O_3 and ZnO/Ag binary systems were used for the degradation of textile dyes under visible light irradiation for 8 h and 4 h respectively.[24,25] This ternary ZnO/Ag/Mn_2O_3 catalyst is found to degrade the industrial textile effluent much faster (*i.e.* 3 h) in comparison to earlier reports, which is a significant improvement.[24,25]

The enhanced visible light photocatalytic activity of ternary ZnO/Ag/Mn_2O_3 nanocomposite depends on several factors such as size, morphology and surface area. The size of the synthesized ternary ZnO/Ag/Mn_2O_3 nanocomposite was small compared with pure ZnO which was evidently shown by TEM and FE-SEM observations. The smaller size of the ternary ZnO/Ag/Mn_2O_3 nanocomposite gives high surface to volume ratio and can also create the possibility of indirect electron transition which in turn generates more number of electrons and holes. In other words, it is known that the photocatalytic redox reaction mainly takes place on the surface of the photocatalysts, so the surface properties significantly influence the efficiency of the catalysts.[34–36] The ternary ZnO/Ag/Mn_2O_3 nanocomposite show higher surface area and smaller size because of the synergetic effect among the components *i.e.* ZnO, Ag and Mn_2O_3.

Another reason for the enhancement of photocatalytic activity is that the ternary ZnO/Ag/Mn_2O_3 nanocomposite containing metallic Ag which has strong electron accepting ability.[24] So the Ag nanoparticles can act as electron traps facilitating the electron–hole separation and subsequent transfer of the trapped electron to the adsorbed O_2 which acts as an electron acceptor on the surface of ZnO and Mn_2O_3. Also, the ternary ZnO/Ag/Mn_2O_3 nanocomposite could have more than one pathway for the formation of electron–hole pairs which is due to three different interfaces and the electron–hole pair recombination is prevented to the maximum extent in the

ternary ZnO/Ag/Mn_2O_3 nanocomposite.[30,37,38] As a result, the ternary ZnO/Ag/Mn_2O_3 catalyst exhibits the higher photocatalytic activity when compared to the binary catalysts (ZnO/Ag, and ZnO/Mn_2O_3) and pure ZnO.[24,25] Therefore, size, shape and surface area of the catalysts were found to play the significant role in achieving higher photocatalytic degradation efficiency within short duration of irradiation time. After a thorough investigation we came to a conclusion that the ternary system provides an efficient way for production of efficient photocatalytic materials.

Electrochemical detections

Sensing of uric acid (UA) and ascorbic acid (AA) was performed by the electrochemical experiments. Fig. 6a and b indicates the cyclic voltammetry (CV) response of 3 mM UA and AA for bare GCE and pure ZnO as well as ternary ZnO/Ag/Mn_2O_3 nanocomposite modified GCE at a scan rate 50 mV s^{-1}. Fig. 6a and b clearly indicates that the ternary ZnO/Ag/Mn_2O_3 nanocomposite is showing higher cathodic current compared with pure ZnO nanorods. This is attributed to the fast electron transfer through the different interfaces in case of ternary ZnO/Ag/Mn_2O_3 nanocomposite compared to pure ZnO. Further the ternary ZnO/Ag/Mn_2O_3 nanocomposite was employed for the detection of different concentrations of UA and AA (1 mM to 8 mM) and the calibration plot is shown by Fig. 7. Fig. 7 indicates that as the concentrations of UA and AA increases, the current response also linearly increases. When compared with bulk ZnO/Ag/Mn_2O_3, the prepared nanosized ternary ZnO/Ag/Mn_2O_3 nanocomposite exhibits high sensitivity for detection of UA and AA which was evidently shown in Fig. S6.† Recently, Suresh *et al.* reported that high availability of surface area increases the active sites, which produces more number of electrons which is favourable for high sensitivity and detection of enzymes.[15]

Based on this report, we concluded that the ternary ZnO/Ag/Mn_2O_3 nanocomposite having high surface area and small size is favourable to exhibit higher current response than that of pure ZnO nanorods. These results are in good agreement with the CV, BET, FE-SEM and TEM analyses.

Antibacterial activity

The procedure of antibacterial activity was followed from previous literatures and it is described in ESI.†[11,39,40] In order to study the antibacterial activities of the pure ZnO and ternary ZnO/Ag/Mn_2O_3 nanocomposite, the synthesized materials were used against the gram positive (*Staphylococcus aureus*) and gram negative (*Escherichia coli*) bacteria. Fig. 8a and b describes comparative antibacterial activities of 1 mM of pure ZnO and ternary ZnO/Ag/Mn_2O_3 nanocomposite which represents zone of inhibition for the growth of gram positive and negative bacteria. Fig. 8 clearly indicates that compared with pure ZnO, the ternary ZnO/Ag/Mn_2O_3 nanocomposite shows much better antibacterial activity and their corresponding zone of inhibition are tabulated in Table 1. The ternary ZnO/Ag/Mn_2O_3 nanocomposite reveals better antibacterial activities due to active oxygen spices, small size and high surface area which was proved by the BET and XPS results. The results reported here are better than the previous reports.[39,40]

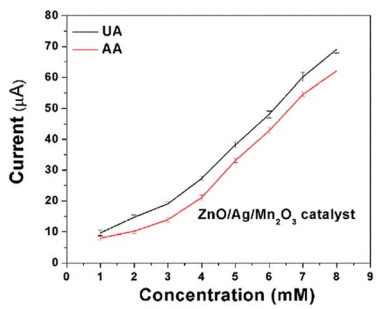

Fig. 7 Current response for different concentrations of UA and AA (1 mM to 8 mM) in the presence of ternary ZnO/Ag/Mn_2O_3 nanocomposite modified GCE.

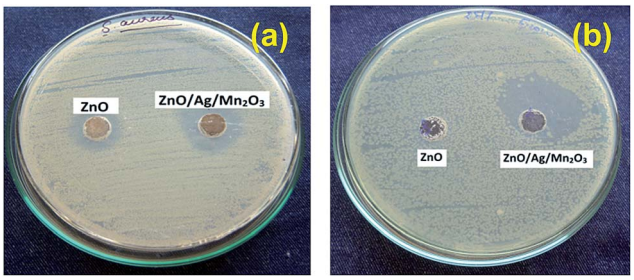

Fig. 8 Photographs represents zone of inhibition by pure ZnO and ternary ZnO/Ag/Mn_2O_3 nanocomposite against (a) *Staphylococcus aureus*, and (b) *Escherichia coli*.

Table 1 Zone of inhibition by 1 mM of pure ZnO and ternary ZnO/Ag/Mn_2O_3 nanocomposite against gram positive and negative bacteria

		Zone of inhibition in mm			
Sample	Bacteria	Trial 1	Trial 2	Trial 3	Average
ZnO	*S. aureus*	13.1	12.8	13.3	13.06
	E. coli	10.2	10.6	10.3	10.36
ZnO/Ag/Mn_2O_3	*S. aureus*	22.1	22.4	22.5	22.33
	E. coli	25.2	25.4	25.1	25.23

Conclusions

This study proposed a thermal decomposition method to synthesize ternary ZnO/Ag/Mn_2O_3 nanocomposite in which the synergistic effect among ZnO, Ag, and Mn_2O_3 could have enhance the response of the nanocomposite to visible light-induced photocatalysis, sensing of uric acid and ascorbic acid, and, antibacterial activities. The improved rapid transfer of electrons and inhibited charge recombination at the interface seems responsible for excellent and enhanced visible light-induced photocatalytic degradation of industrial textile effluent and sensing of uric acid and ascorbic acid. The antimicrobial experiments showed that the ternary ZnO/Ag/Mn_2O_3 nanocomposite have considerable bactericidal activity due to the presence of Ag, small size, high surface area and synergistic effect between the

ZnO, Ag, and Mn_2O_3. The visible light photocatalysis, sensing and antimicrobial activity confirmed that the ternary ZnO/Ag/Mn_2O_3 nanocomposite is a very valuable material that can be used for a range of applications. This paper reports an approach to synthesize novel and useful materials for multiple uses.

Acknowledgements

We acknowledge National Centre for Nanoscience and Nanotechnology, University of Madras, Chennai, India for XPS and TEM characterizations. The authors (R.S., F.G.) acknowledge the support of CONICYT through the project CONICYT/FONDAP/15110019 and the postdoctoral fellowship granted to R.S.

Notes and references

1 Investing in water and sanitation: Increasing access, reducing inequalities UN-water global analysis and assessment of sanitation and drinking-water GLASS 2014.
2 World water assessment programme: Water for people, water for life: The UN-world water development development report UNESCO-WWAP 2003.
3 V. K. Gupta, I. Ali, T. A. Saleh, A. Nayak and S. Agarwal, *RSC Adv.*, 2012, **2**, 6380.
4 J. Liqiang, S. Xiaojun, S. Jing, C. Weimin, X. Zili, D. Yaguo and F. Honggang, *Sol. Energy Mater. Sol. Cells*, 2003, **79**, 133.
5 N. Chaniotakis and N. Sofikiti, *Anal. Chim. Acta*, 2008, **615**, 1.
6 A. Fujishima and K. Honda, *Nature*, 1972, **238**, 37.
7 M. M. Khan, S. A. Ansari, M. I. Amal, J. Lee and M. H. Cho, *Nanoscale*, 2013, **5**, 4427.
8 M. M. Khan, S. A. Ansari, M. O. Ansari, B. K. Min, J. Lee and M. H. Cho, *J. Phys. Chem. C*, 2014, **118**, 9477.
9 M. M. Khan, S. A. Ansari, D. Pradhan, D. H. Han, J. Lee and M. H. Cho, *Ind. Eng. Chem. Res.*, 2014, **53**, 9754.
10 M. M. Khan, J. Lee and M. H. Cho, *J. Ind. Eng. Chem.*, 2014, **20**, 1584.
11 M. M. Khan, S. A. Ansari, J. H. Lee, M. O. Ansari, J. Lee and M. H. Cho, *J. Colloid Interface Sci.*, 2014, **431**, 255.
12 S. A. Ansari, M. M. Khan, M. O. Ansari, J. Lee and M. H. Cho, *J. Phys. Chem. C*, 2013, **117**, 27023.
13 S. G. Ansari, *et al.*, *Sens. Actuators, B*, 2009, **137**, 566.
14 S. M. Usman Ali, N. H. Alvi, Z. Ibupoto, O. Nur, M. Willander and B. Danielsson, *Sens Actuators, B*, 2011, **152**, 241.
15 R. Suresh, K. Giribabu, R. Manigandan, A. Stephen and V. Narayanan, *RSC Adv.*, 2014, **4**, 17146.
16 R. Saravanan, V. K. Gupta, V. Narayanan and A. Stephen, *J. Mol. Liq.*, 2013, **181**, 133.
17 R. Ahmad, N. Tripathy, N. K. Jang, G. Khang and Y. B. Hahn, *Sens. Actuators, B*, 2015, **206**, 146.
18 C. Xia, W. Ning, W. Long and G. Lin, *Sens. Actuators, B*, 2010, **147**, 629.
19 R. Ullah and J. Dutta, *J. Hazard. Mater.*, 2008, **156**, 194.
20 Y. Jiang, Y. Sun, H. Liu, F. Zhu and H. Yin, *Dyes Pigm.*, 2008, **78**, 77.
21 Q. Yu, J. Li, H. Li, Q. Wang, S. Cheng and L. Li, *Chem. Phys. Lett.*, 2012, **539**, 74.
22 S. Anandan, N. Ohashi and M. Miyauchi, *Appl. Catal., B*, 2010, **100**, 502.
23 R. Saravanan, H. Shankar, T. Prakash, V. Narayanan and A. Stephen, *Mater. Chem. Phys.*, 2011, **125**, 277.
24 R. Saravanan, N. Karthikeyan, V. K. Gupta, P. Thangadurai, V. Narayanan and A. Stephen, *Mater. Sci. Eng., C*, 2013, **33**, 2235.
25 R. Saravanan, V. K. Gupta, V. Narayanan and A. Stephen, *J. Taiwan Inst. Chem. Eng.*, 2014, **45**, 1910.
26 R. Saravanan, E. Thirumal, V. K. Gupta, V. Narayanan and A. Stephen, *J. Mol. Liq.*, 2013, **177**, 394.
27 Z. W. Pan, Z. R. Dai and Z. L. Wang, *Science*, 2001, **291**, 1947.
28 K. Jayanthi, S. Chawla, K. N. Sood, M. Chhibara and S. Singh, *Appl. Surf. Sci.*, 2009, **255**, 5869.
29 T. He, Z. Zhou, W. Xu, Y. Cao, Z. Shi and W. P. Pan, *Compos. Sci. Technol.*, 2010, **70**, 1469.
30 H. Wang, S. Baek, J. Lee and S. Lim, *Chem. Eng. J.*, 2009, **146**, 355.
31 S. Yuana, P. Mklaudeau and V. Pemchon, *Appl. Catal., B*, 1994, **3**, 319.
32 M. S. P. Francisco, V. R. Mastelaro, P. A. P. Nascente and A. O. Florentino, *J. Phys. Chem. B*, 2001, **105**, 10515.
33 J. Mu, C. Shao, Z. Guo, Z. Zhang, M. Zhang, P. Zhang, B. Chen and Y. Liu, *ACS Appl. Mater. Interfaces*, 2011, **3**, 590.
34 X. Yang, Y. Wang, L. Xu, X. Yu and Y. Guo, *J. Phys. Chem. C*, 2008, **112**, 11481.
35 J. M. Hermann, J. Disdier and P. Pichat, *J. Phys. Chem.*, 1986, **90**, 6028.
36 A. Sclafani and J. M. Hermann, *J. Photochem. Photobiol., A*, 1998, **113**, 181.
37 H. M. Sung-suh, J. R. Choi, H. J. Hah, S. M. Koo and Y. C. Ba, *J. Photochem. Photobiol., A*, 2004, **163**, 37.
38 L. Ge, M. Xu and H. Fang, *J. Mol. Catal. A: Chem.*, 2006, **258**, 68.
39 L. Zhang, Y. Jiang, Y. Ding, M. Povey and D. York, *J. Nanopart. Res.*, 2007, **9**, 479.
40 O. Yamamoto, J. Sawai and T. Sasamoto, *Int. J. Inorg. Mater.*, 2000, **2**, 451.